Characterization of proton and heavier ion acceleration in ultrahigh-intensity laser interactions with heated target foils

P. McKenna,[1,*] K. W. D. Ledingham,[1,†] J. M. Yang,[1,‡] L. Robson,[1,†] T. McCanny,[1] S. Shimizu,[1,§] R. J. Clarke,[2] D. Neely,[2] K. Spohr,[3] R. Chapman,[3] R. P. Singhal,[4] K. Krushelnick,[5] M. S. Wei,[5] and P. A. Norreys[2]

[1]*Department of Physics, University of Strathclyde, Glasgow G4 0NG, United Kingdom*

[2]*Central Laser Facility, Rutherford Appleton Laboratory, Chilton, Didcot, Oxon OX11 0QX, United Kingdom*

[3]*Department of Electronic Engineering and Physics, University of Paisley, PA1 2BE, United Kingdom*

[4]*Department of Physics and Astronomy, University of Glasgow, Glasgow G12 8QQ, United Kingdom*

[5]*Blackett Laboratory, Imperial College, London SW7 2BZ, United Kingdom*

(Received 2 April 2004; published 21 September 2004)

Proton and heavy ion acceleration in ultrahigh intensity ($\sim 2\times 10^{20}$ W cm^{-2}) laser plasma interactions has been investigated using the new petawatt arm of the VULCAN laser. Nuclear activation techniques have been applied to make the first spatially integrated measurements of both proton and heavy ion acceleration from the same laser shots with heated and unheated Fe foil targets. Fe ions with energies greater than 10 MeV per nucleon have been observed. Effects of target heating on the accelerated ion energy spectra and the laser-to-ion energy conversion efficiencies are discussed. The laser-driven production of the long-lived isotope ^{57}Co (271 days) via a heavy ion induced reaction is demonstrated.

DOI: 10.1103/PhysRevE.70.036405 PACS number(s): 52.70.Nc, 25.70.Gh, 25.70.Hi, 25.70.Jj

I. INTRODUCTION

The acceleration of high quality ion beams in the interaction of high-intensity laser pulses with dense plasma is generating considerable international interest at present [1,2]. In recent studies the production of high acceleration fields of the order of MV/μm has been demonstrated and this has given rise to bright, pulsed, low emittance beams of protons with energies up to 58 MeV [1] and heavier ions (C, F, Al, and Pb) with up to 7 MeV per nucleon [3–5]. Measurements of these ions have been used to diagnose high density plasma processes, including ionization and acceleration, and accelerated protons have also been shown to provide a time-dependent probe of electric fields [6]. Suggested applications for this potentially compact laser-plasma-based ion source include isotope production for nuclear medicine [7], injectors for future large-scale ion accelerators [8], and fast ion-based fast ignitor schemes [9].

Thomson parabola ion spectrometers and nuclear activation techniques have been successfully employed to measure the acceleration of fast protons and recently heavy ions in intense laser-interaction physics [3–5]. Whereas the former technique supports simultaneous measurement of ion charge states and energy distributions, it is limited to sampling a small solid angle (typically $\sim 10^{-5}$ sr). Activation techniques can however provide a measurement of the integrated ion flux over a large solid angle. This is important as the ion expansion profile in some situations is influenced by self-generated electric and magnetic fields in the plasma [3]. Whereas proton-induced reactions have been widely used to diagnose proton acceleration [7], nuclear activation techniques have only recently been developed for measurements of laser-plasma driven "heavy" ion acceleration [5]. McKenna *et al.* [5] have shown that fusion reactions between fast heavy ions from a laser-produced plasma and stationary atoms in an adjacent "activation" sample create compound nuclei in excited states, which de-excite through the evaporation of protons, neutrons, and α-particles. The emission of precise energy γ-rays from the residual nuclei in the activated samples were measured and used with calculated reaction cross sections to make quantitative measurements of heavy ion acceleration from a laser-produced plasma.

Experiments employing Thomson parabola ion spectrometers have shown that in addition to the acceleration of constituent heavy ions from a target foil, hydrocarbon and H_2O contaminants on the surfaces of the target are also ionized and accelerated, and result in the production of beams of protons and carbon and oxygen ions [3–5]. These contaminants arise due to the poor vacuum conditions (typically $\sim 10^{-4}$ Torr) under which experiments of this nature are routinely performed. Due to their higher charge-to-mass ratio, parasitic protons are more efficiently accelerated than any other ion species and effectively screen the acceleration potential, reducing the efficiency of heavier ion acceleration. It has also been shown, using Thomson parabola spectrometers and CR-39 plastic track detectors, that sufficient heating of the solid target removes contamination layers increasing the numbers of heavier ions accelerated [4,10]. The application of nuclear activation techniques to quantify ion acceleration from moderately heated targets demonstrated, for an Al foil target heated to $\sim 400\,^{\circ}$C, a reduction in the accelerated proton flux and the production of heavy ion fusion-evaporation reactions, which were not observed with the unheated target [11].

*Electronic mail: p.mckenna@phys.strath.ac.uk

†Also at AWE plc Aldermaston, Reading RG7 4PR, UK.

‡Present address: Research Center of Laser Fusion, P.O. Box 919-986, Mianyang, 621900, People's Republic of China.

§Present address: Institute for Chemical Research, Kyoto University, Gokasho, Uji, Kyoto 611-0011, Japan.

 ©2004 The American Physical Society

In this paper, nuclear activation techniques have been further developed and applied to make the first comparison of spatially integrated ion flux measurements of proton and heavy ion acceleration from the same laser shots with heated and unheated targets. Due to its high melting point, Fe was chosen as the target foil and heated to temperatures in excess of 850 °C. The relatively high mass of Fe compared to the surface contaminant species (H, C, and O) removes any ambiguity in identifying heavy ion induced reaction channels in the surrounding activation samples. Furthermore, carbon was chosen as the activation material to facilitate the observation of a large number of residual nuclei with suitable half-lifes, from fusion-evaporation reactions with cross sections in the ion energy range of interest. The derived energy distributions of the accelerated protons and heavy ions from petawatt-class laser-plasma interactions are presented. The energy spectra and energy conversion efficiency values are compared with measurements using unheated targets in otherwise identical conditions.

II. EXPERIMENT

The recently developed petawatt arm of the VULCAN Nd:glass laser at the Rutherford Appleton Laboratory, UK, was used in this experiment. *p*-polarized laser pulses with energy up to 400 J, wavelength ~ 1 μm and average duration 0.7 ps, were focused onto foil targets at an angle of 45° and to a peak intensity of the order of 2×10^{20} Wcm^{-2}. No direct measurement of the temporal profile of the rising edge of the laser pulse is available. However, a 20 GHz photodiode coupled to a 6 GHz LeCroy digital storage oscilloscope was used, with appropriate filtering and on full energy laser shots, to measure the level of any amplified spontaneous emission (ASE) or prepulse activity. An intensity contrast measurement of over 7 orders of magnitude was achieved and at this level no prepulses were observed within a 10 ns period prior to the main pulse. The upper limit of the ASE or prepulse intensity for this experiment was therefore $\sim 10^{13}$ Wcm^{-2}.

100-μm-thick, 5 mm$\times$5 mm, Fe foil targets were irradiated to generate multi-MeV proton and heavier ion beams. Prior to several of the laser shots the foil target was resistively heated to a temperature of 860 °C for $\sim$30 min. The foil temperature was monitored using a thermocouple.

Ion acceleration from the heated and unheated targets was diagnosed via ion induced reactions in activation materials surrounding the Fe target. 1-mm-thick, 5 cm$\times$5 cm carbon activation samples were positioned along the target normal direction at both the front and rear of the target, as shown in Fig. 1, and used to measure ^{56}Fe acceleration via the production of ^{56}Fe+^{12}C fusion–evaporation reactions. The carbon activation samples each subtended a solid angle of 1 sr. After each laser shot, two well-shielded germanium detectors (with relative efficiencies of 25% and 35% compared to the 3 in. $\times$3 in. NaI standard) were used to measure the characteristic γ rays emitted by residual nuclei, produced through the evaporation of protons, neutrons and α particles from the ^{56}Fe+^{12}C compound nucleus. As laser irradiation of the target took place under vacuum conditions ($<10^{-4}$ mbar), a period of about 15 min was required to remove the activated material from the target chamber, thus limiting the measurement to the detection of γ emission from nuclides with half-lifes greater than a few minutes. The residual nuclides and corresponding reactions produced in the carbon samples were identified by the measured γ energies, intensities, and half-lifes.

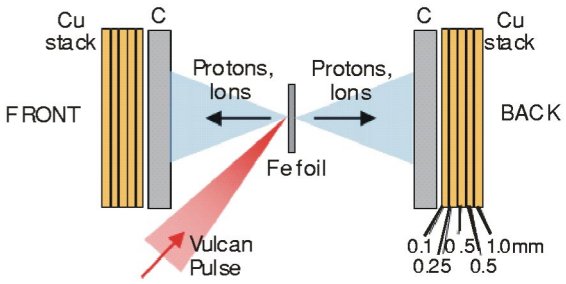

FIG. 1. (Color online) Experimental arrangement used for diagnosing ion acceleration using nuclear activation techniques.

Proton acceleration was diagnosed via proton induced reactions in copper. A stack of copper foils was positioned directly behind each of the carbon samples, as shown in Fig. 1. The copper pieces were 50 mm$\times$50 mm and ranged in thickness from 100 μm (front of each stack) to 1 mm (rear of each stack). The activity of the positron emitter ^{63}Zn, produced from (p,n) reactions on ^{63}Cu, was measured for each copper foil using NaI detectors operated in coincidence and set to detect the two 511 keV photons signature of positron annihilation.

A similar technique was employed to determine both the proton and Fe ion energy spectra and involved a convolution of the measured number of reactions induced, the reaction cross sections (as a function of ion energy) and the ion stopping powers in the activation targets (also a function of ion energy).

III. RESULTS

In the first part of the experiment an unheated Fe foil was irradiated with a 233 J laser pulse. Figure 2(a) shows a typical region of interest in the γ emission spectra detected from the carbon sample positioned at the front side of the target. The detected peaks have been identified as resulting from the decay of ^{63}Zn, ^{66}Ga, ^{66}Ge, ^{65}Ga, ^{61}Cu, ^{60}Cu, and ^{44}Sc. The evaporation reactions from the compound ^{56}Fe+^{12}C nucleus giving rise to these nuclei and the corresponding reaction energy thresholds are listed in Table I. The numbers of each observed nucleus produced at the time of the laser shot are also listed. These have been determined from the characteristic line intensities in five spectra measured during the 24 h period after the laser shot, and have been corrected for detection efficiencies, decay branching ratios, γ emission probabilities, and half-lifes. The carbon sample at the rear side of the unheated target showed no characteristic peaks corresponding to any ^{56}Fe+^{12}C fusion evaporation reactions and therefore it is concluded that within the dynamic range of this diagnostic technique there are no ^{56}Fe ions accelerated from the rear of the cold target.

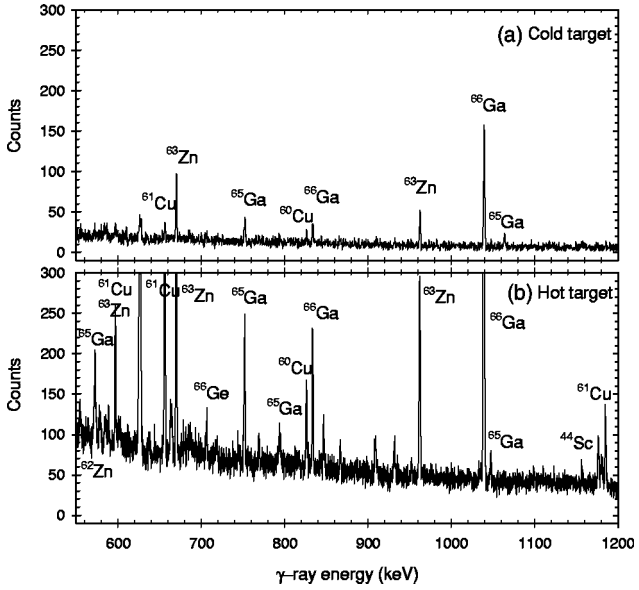

FIG. 2. Part of the γ-ray spectrum from carbon activation samples positioned at the front of the Fe foil target, which was (a) unheated and (b) heated to 860 °C. The counting time for each spectrum was ~3 h. The half-lifes of the reaction products were determined by repeating the measurements at regular intervals over a 24 h period after the laser shots. Fusion–evaporation reactions giving rise to the observed peaks are listed in Table I.

With a similar Fe foil target heated to 860 °C and irradiated with a 274 J laser pulse, additional fusion–evaporation reactions were induced (as listed in Table I), in a new carbon sample at the front. These have resulted in the detection of additional signature γ emission peaks from the production of ^{67}Ga, ^{67}Ge, ^{62}Zn, ^{57}Co, ^{56}Mn, ^{52}Mn, ^{52m}Mn, ^{49}Cr, ^{55}Co, and ^{44m}Sc, as shown in Fig. 2(b). As with the cold target, no ^{56}Fe-induced fusion–evaporation reactions were observed in the C sample positioned at the rear of the heated target foil, again indicating that above the detection threshold for this technique no constituent heavy ions were accelerated at the rear of the 100-μm-thick Fe foil. This result is in direct contrast with measurements of heavy ion acceleration from heated 50-μm-thick Al and W foil targets performed with the 100 TW laser at the Laboratoire pour l'Utilisation des Lasers Intenses (LULI) [4], in which source layers of C and F atoms were ionized and accelerated from the rear of the target.

In addition to the observed residual nuclei resulting from ^{56}Fe+^{12}C fusion reactions (Table I), a signature peak of ^{24}Na was detected in both the front and rear carbon samples, for both the hot and cold target shots. ^{24}Na is produced by the acceleration of contaminant oxygen ions giving rise to the reaction $^{16}O+^{12}C \rightarrow ^{24}Na+1n+3p$. Although the signature for this reaction was much stronger in the front sample, the fact that this nuclei was also detected in the rear sample indicates that surface contamination atoms heavier than hydrogen can still be ionized and accelerated at the rear. It is interesting to note that the level of this signal increased by about a factor of 2 when the target was heated, indicating

TABLE I. The residual nuclei observed in the C activation samples at the front of the laser irradiated heated and unheated Fe foil targets. The ^{56}Fe+^{12}C fusion–evaporation reactions and threshold energies, E_{thresh}, for each reaction are listed. The numbers of each nuclei, per laser shot, have been determined after correction for detection efficiencies, decay branching ratios, γ emission probabilities, and half-lifes.

Observed nuclei	Evaporation reactions	E_{thresh} (MeV)	Principal measured γ(keV)	Literature half-life	Measured half-life (860 °C)	Numbers of nuclei	
						Unheated	860 °C
^{67}Ga	$1p$	1.2	93.3	3.3 d	—	—	3.5×10^5
^{67}Ge	$1n$	9.8	167.0	18.7 min	26.5 min	—	3.9×10^4
^{63}Zn	$1\alpha+1n$	10.6	669.6	38.9 min	38.5 min	3.8×10^5	2.1×10^6
^{66}Ga	$1n+1p$	14.7	1039.2	9.5 h	9.9 h	6.4×10^5	3.8×10^6
^{66}Ge	$2n$	18.2	43.9	2.3 h	2.2 h	6.2×10^4	4.4×10^5
^{62}Zn	$1\alpha+2n$	21.7	596.6	9.3 h	9.4 h	—	6.9×10^5
^{65}Ga	$2n+1p$	25.7	115.1	15.2 min	13.6 min	2.1×10^5	1.6×10^6
^{61}Cu	$1\alpha+2n+1p$	29.4	283.0	3.4 h	3.3 h	2.0×10^5	1.3×10^6
^{57}Co	$2\alpha+2n+1p$	35.6	122.0	271.4 d	—	—	1.2×10^6
^{60}Cu	$1\alpha+3n+1p$	43.6	1333.0	24.4 min	23.7 min	7.6×10^4	2.8×10^5
^{56}Mn	$2\alpha+1n+3p$	46.2	846.8	2.6 h	—	—	2.3×10^4
^{52}Mn	$3\alpha+3n+1p$	58.5	935.5	5.6 d	—	—	3.2×10^5
^{52m}Mn	$3\alpha+3n+1p$	58.5	1434.1	21.1 min	—	—	3.1×10^4
^{49}Cr	$4\alpha+3n$	59.2	90.6	41.9 min	35.0 min	—	4.7×10^4
^{55}Co	$2\alpha+4n+1p$	61.3	931.5	17.5 h	—	—	6.8×10^4
^{44}Sc	$5\alpha+3n+1p$	79.9	1157.0	3.9 h	—	2.3×10^4	1.9×10^4
^{44m}Sc	$5\alpha+3n+1p$	79.9	271.1	2.4 d	—	—	1.2×10^5

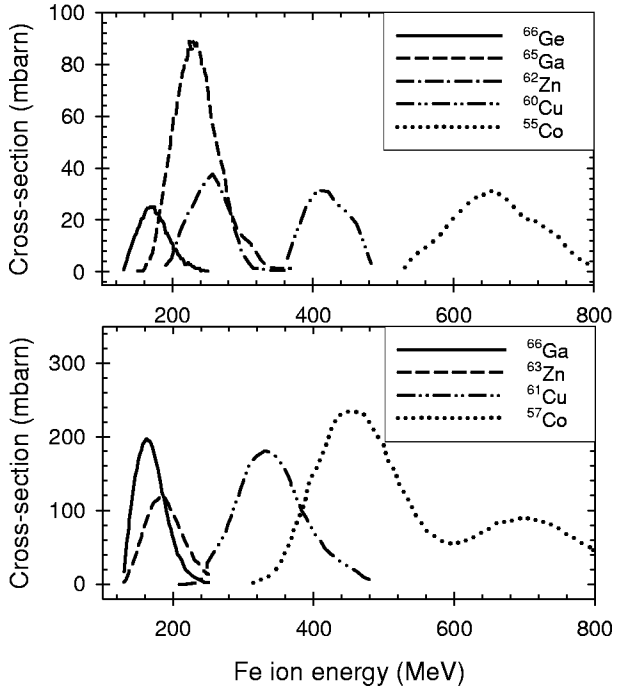

FIG. 3. Cross sections for ^{56}Fe+^{12}C fusion–evaporation reactions leading to the production of ^{66}Ge, ^{65}Ga, ^{62}Zn, ^{60}Cu, ^{55}Co, ^{66}Ga, ^{63}Zn, ^{61}Cu, and ^{57}Co. The cross sections have been calculated using the PACE-2 Monte Carlo code.

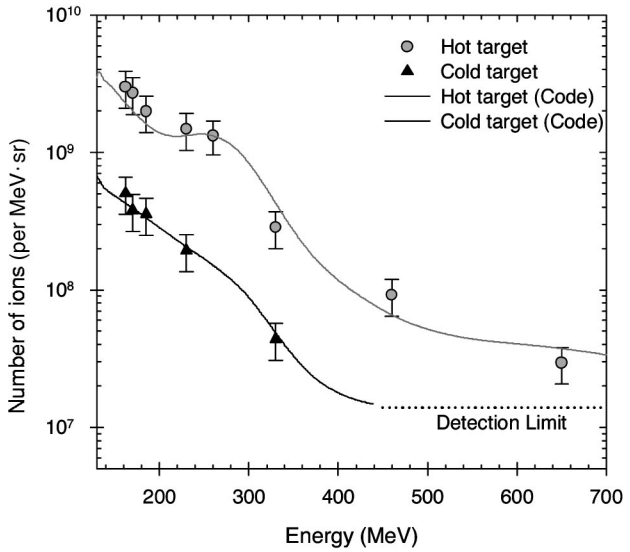

FIG. 4. Fe ion energy distribution, deduced by determining the numbers of ions (with energy above the reaction threshold energy) required to induce the measured activities of the ^{66}Ge, ^{65}Ga, ^{62}Zn, ^{66}Ga, ^{63}Zn, ^{61}Cu, and ^{57}Co nuclides. ^{60}Cu was not used in the calculations due to possible cascade contributions from the production of ^{60m}Co, for which cross sections were not available. The black and gray points result from calculations performed for each observed reaction with the Fe foil target unheated and heated to 860 °C respectively. The black and gray lines are the corresponding results of the full convolution involving all the above reactions. The detection limit for the technique was determined to be $\sim 10^7$ ions/MeV in the high energy range.

that not all of the surface contamination was removed and that heavier *contaminant* ions are also more efficiently accelerated with target heating to remove parasitic protons.

As discussed in detail elsewhere [5], observed residual nuclides for which the reaction process and mode of decay have been identified can be used to quantify ion acceleration. This is possible because all of the heavy ions are stopped in the activation sample. The technique involves a convolution of the ion stopping ranges in the sample and the reaction cross sections as a function of energy. Cross sections for the observed fusion–evaporation reactions were calculated using the Monte Carlo code PACE-2 [12]. PACE-2 calculates total fusion cross sections for a compound nucleus system and incorporates atomic masses from the Audi/Wapstra tables [13] to calculate yields for fission exit channels. For each ^{56}Fe+^{12}C fusion–evaporation reaction leading to an observed nucleus listed in Table I, 10 000 fusion events were simulated in 2 MeV steps, to calculate the energy dependent cross sections shown in Fig. 3. The PACE-2 calculations have an overall accuracy of between 10% and 20%. Importantly, the cross sections for the observed reactions extend over a wide range of Fe ion energies, which defines the energy range over which the energy spectrum can be unfolded. The stopping powers of Fe ions in C were determined using the SRIM-2003 [14] Monte Carlo code, which calculates the interactions of ions in matter using a quantum mechanical treatment of ion–atom collisions.

Two techniques were used to convolute the calculated cross sections and stopping powers, with the measured numbers of each reaction, to determine the Fe ion energy spectra. First, a rudimentary calculation was performed using a simplified "flat-top" cross section with a value of half the PACE-2 cross section peak (but with a similar integral cross section) to determine the numbers of ions/MeV contributing to an observed reaction. This calculation involved using the range of the ions in the activation target, the number density of the target and the measured number of reactions, as listed in Table I. The calculation was repeated for each of the observed reactions, with cross sections peaked at different projectile ion energies, and resulted in the discrete points in the energy distribution shown in Fig. 4, where each point is calculated by considering a separate reaction process. The calculations were performed for both the hot and cold target results. Second, a code was developed to convolute the various parameters for all of the reactions to unfold the full incident Fe ion energy spectra in small energy steps of 0.5 MeV. The method involves a convolution of the calculated cross sections and stopping powers to derive a "response function," which determines the numbers of each reaction (and hence each residual nucleus) produced by a Fe ion at a given energy. Starting with an arbitrary initial Fe ion energy spectrum, the numbers of each residual nucleus were calculated by convoluting the energy spectrum with the response function for each reaction. The Fe ion energy spectrum was then iteratively adjusted and the calculation repeated until the difference in the calculated and the measured number of residual nuclides was minimized. The results are plotted as lines in Fig. 4 for both the hot and cold target shots. There is excellent agreement in the quantities of ions

and the overall shapes of the energy spectra unfolded using both techniques. Errors bars have been plotted at 30% uncertainty level, with the largest contribution arising from the uncertainty in the calculated cross section. It should be noted that the effect of the isotopic abundance of the target Fe foil [^{56}Fe (91.8%); ^{54}Fe (5.8%); ^{57}Fe (2.1%); ^{58}Fe (0.3%)] was determined. In addition to the cross section calculations for ^{56}Fe+^{12}C fusion reactions, the PACE-2 code was also used to calculate cross sections for ^{54}Fe+^{12}C reactions leading to the same observed residual nuclei. The ion spectra were calculated firstly using only the ^{56}Fe cross sections and then using ^{56}Fe and ^{54}Fe cross sections weighted to the isotopic abundances. The additional stable isotope had little effect on the final output ion spectra.

As shown in Fig. 4, for the unheated target the Fe ion numbers decrease from $\sim 5\times 10^8$ ions/MeV at low energies ($\sim$150 MeV) to $\sim 10^7$ ions/MeV at $\sim$400 MeV, with a corresponding conversion efficiency from laser energy to Fe ion acceleration (with energy above $\sim$150 MeV) of ~0.8%. With the Fe target heated to 860 °C the numbers of Fe ions accelerated over the observed energy range is up to an order of magnitude higher and corresponds to an energy conversion efficiency of $\sim$4.2%. It should be noted that the calculated energy conversion efficiency involves ^{56}Fe ions in the energy range of the observed nuclear reactions and contributing to the nuclear reactions. The total energy conversion efficiency to heavy ion acceleration over the full energy range and including the acceleration of any remaining surface contaminant species will be higher. It is clear from these spatially integrated ion flux measurements that heating the primary target has the effect of increasing the efficiency of heavy ion acceleration, in line with previous results using an ion spectrometer to sample a small solid angle [4,10]. It is also noted that Fe ions have been accelerated to energies in excess of 10 MeV per nucleon for the heated target shot.

The additional nuclei observed with the hot target (Table I) are produced due to a higher flux of higher energy ions compared with the cold Fe target. The reactions leading to the production of ^{55}Co and ^{57}Co, for example, both have relatively high cross section values at high incident ion energies. Measurements of these reaction products have facilitated quantification of the ^{56}Fe energy spectrum to 700 MeV for the heated target result. No ^{56}Fe ions were detected, above the detection limit, in this energy region for the cold target shot.

The lower detection limit of this diagnostic technique is defined by the ability to resolve signature γ-ray peaks against a background continuum level (Fig. 2 shows a typical spectrum). The background level varies as a function of γ energy and the sample activity (which is time dependent). The ability to resolve a peak also depends on the detection efficiency (γ energy dependent) and the total counting time for the measurement. Since the residual nuclei produce γ rays with a range of energies and emission probabilities, and have reaction cross sections peaked at different ion energies, the lower limit of detection for this diagnostic varies across the ion energy distribution. Using detection of a ^{55}Co signature γ emission (931.5 keV) as an example, the lower detection limit has been determined to be $\sim 10^7$ ions(/MeV) in the high energy range $\sim$650 MeV.

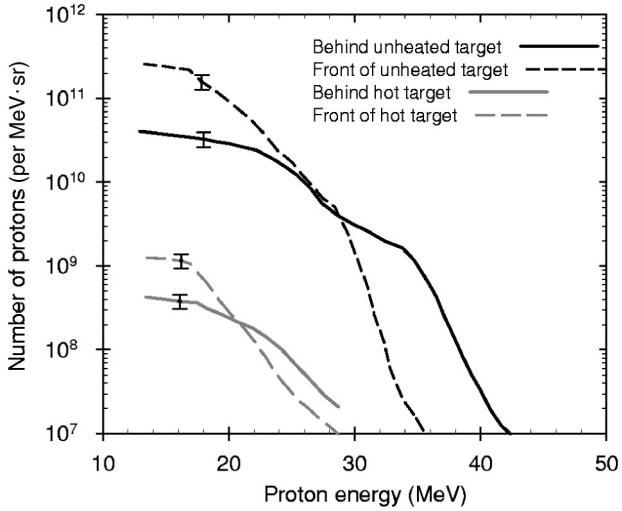

FIG. 5. Proton energy spectra determined from measured ^{63}Cu$(p,n)^{63}$Zn reactions in stacks of Cu foils. The proton flux from the heated target (gray lines), measured at both the front (broken lines) and rear (solid lines) of the Fe target foil, is reduced by about 2 orders of magnitude compared to the unheated target (black lines). Typical error bars for the lines are shown.

Proton acceleration from the front and rear surfaces of the Fe target foils was also diagnosed for the same heated and unheated shots by measuring (p,n) reactions in ^{63}Cu. The proton energy spectra were deduced by convoluting the literature cross section for the ^{63}Cu$(p,n)^{63}$Zn reaction [15] and the SRIM-2003 calculated proton stopping ranges in Cu. The technique is described in detail elsewhere [7]. The deduced proton spectra are shown in Fig. 5, and have been corrected for the protons passing through the 1-mm-thick carbon sample (Fig. 1). The measurement was limited to protons with energy above $\sim$13 MeV. As observed in previous experiments [7] the proton maximum cutoff energy is lower for the protons measured at the front side of the target. Significantly, the numbers of protons accelerated from both the front and rear surfaces of the heated target are reduced by about 2 orders of magnitude compared to the unheated target. The energy conversion efficiency to protons in this energy range is of the order of 2% for the unheated target, falling to $\sim$0.01% for the heated target. The total energy conversion efficiency to protons (over the full proton energy range) from unheated targets under similar experimental conditions was measured to be about 7%.

IV. CONCLUSIONS

In summary, the effect of target heating on the acceleration of ions in ultrahigh intensity laser–plasma interactions has been diagnosed via measurements of ion induced nuclear reactions, which sample the spatially integrated flux of ions. Analysis of the reaction products indicates that heating a 100-μm-thick Fe target foil to temperatures in excess of 850 °C removes hydrogen-containing contamination layers, reducing the efficiency of proton acceleration by greater than 2 orders of magnitude and significantly increasing the efficiency of heavy ion acceleration.

It has been clearly demonstrated that through the suitable choice of activation materials, a range of nuclear reactions with cross sections extending throughout the accelerated ion energy range can be induced and used to make spatially integrated measurements of ion acceleration driven by petawatt-class lasers. The technique benefits from a large dynamic range with a lower limit of sensitivity of $\sim 10^7$ ions(/MeV) at high energies. As counting is carried out off-line, the technique is also insensitive to electrical noise generated by the laser-plasma interaction.

High intensity laser-plasma interactions provide a unique and potentially important source of nuclear radiation for the production of radioisotopes. It has been shown that by controlling the target conditions and hence the accelerated ion beam properties, the production of radioisotopes can effectively be controlled. This is highlighted in the present study by the removal of target contamination leading to the first observation of long-lived isotopes such as ^{57}Co (271 day half-life) via a laser-plasma driven process. ^{57}Co could be more efficiently produced via a $^{48}\mathrm{Ti}+{}^{12}\mathrm{C}\rightarrow{}^{57}\mathrm{Co}+2n+1p$ reaction. PACE-2 code calculations were performed to show that the $^{48}\mathrm{Ti}+{}^{12}\mathrm{C}$ reaction has a peaked cross section of 440 mbarns at a relatively low ion energy of $\sim$160 MeV, compared to the cross section peak of 230 mbarns at the higher energy of 450 MeV for the $^{56}\mathrm{Fe}+{}^{12}\mathrm{C}$ reaction (Fig. 3). Experiments with a heated ^{48}Ti target foil in combination with a ^{12}C activation sample would therefore be expected to produce a much greater quantity of the long-lived isotope ^{57}Co. In this way the target and sample combination can be tailored for selective isotope production. This unique radiation source could potentially be used to produce isotopes in other parts of the table of nuclides, which may be more difficult to produce using conventional techniques on large scale nuclear and accelerator facilities.

ACKNOWLEDGMENTS

The authors acknowledge the expert assistance of the VULCAN laser and target area operations teams. P.McK. is supported by a Royal Society of Edinburgh/SEELLD Research Fellowship. J.M.Y. acknowledges support from the China Scholarship Council and S.S. acknowledges support from the Japan Society for the Promotion of Science. This work is funded by the EPSRC (UK).

[1] See, J. T. Mendonca, J. R. Davies, and M. Eloy, Meas. Sci. Technol. **12**, 1801 (2001), and references therein.
[2] K. W. D. Ledingham, P. McKenna, and R. P. Singhal, Science **300**, 1107 (2003).
[3] E. L. Clark *et al.*, Phys. Rev. Lett. **85**, 1654 (2000).
[4] M. Hegelich *et al.*, Phys. Rev. Lett. **89**, 085002 (2002).
[5] P. McKenna *et al.*, Phys. Rev. Lett. **91**, 075006 (2003).
[6] M. Borghesi *et al.*, Phys. Rev. Lett. **88**, 135002 (2002).
[7] I. Spencer *et al.*, Nucl. Instrum. Methods Phys. Res. B **183**, 449 (2001); M. I. K. Santala *et al.*, Appl. Phys. Lett. **78**, 19 (2001).
[8] K. Krushelnick *et al.*, IEEE Trans. Plasma Sci. **28**, 1184 (2000).
[9] M. Roth *et al.*, Phys. Rev. Lett. **86**, 436 (2001).
[10] M. Zepf *et al.*, Phys. Rev. Lett. **90**, 064801 (2003).
[11] P. McKenna *et al.*, Appl. Phys. Lett. **83**, 2763 (2003).
[12] A. Gavron, Phys. Rev. C **21**, 230 (1980).
[13] G. Audi and A. H. Wapstra, Nucl. Phys. A **595**, 409 (1995).
[14] J. F. Ziegler, J. P. Biersack, and U. Littmark, *The Stopping Powers and Ranges of Ions in Solids* (Pergamon, New York, 1985).
[15] EXFOR cross section data online at http://www.nea.fr/html/dbdata/x4/welcome.htm